CHIN. PHYS. LETT. Vol. 38, No. 2 (2021) 027501

Rational Design of Two-Dimensional Magnetic Chromium Borides Based on First-Principles Calculation

Yi-Lin Zhang(张奕林)[1,2], Yue-Yu Zhang(张越宇)[3], Jin-Yang Ni(倪斤阳)[1,2], Ji-Hui Yang(杨吉辉)[1,2*], Hong-Jun Xiang(向红军)[1,2], and Xin-Gao Gong(龚新高)[1,2*]

[1]*Key Laboratory of Computational Physical Sciences (Ministry of Education), State Key Laboratory of Surface Physics, and Department of Physics, Fudan University, Shanghai 200433, China*
[2]*Collaborative Innovation Center of Advanced Microstructures, Nanjing 210093, China*
[3]*Department of Chemistry, Imperial College London, W12 0BZ, United Kingdom*

(Received 1 December 2020; accepted 17 December 2020; published online 27 January 2021)

Two-dimensional (2D) magnetic materials have been experimentally recognized recently, however, the Curie temperatures (T_C) of known 2D systems are quite low. Generally, magnetic systems can be seen as constituent magnetic elements providing spins and the non-magnetic elements providing frameworks to host the magnetic elements. Short bond lengths between the magnetic and non-magnetic elements would be beneficial for strong magnetic interactions and thus high T_C. Based on this, we propose to combine the magnetic element Cr and the non-magnetic element boron to design novel 2D magnetic systems. Using our self-developed software package IM^{2}ODE, we design a series of chromium-boride based 2D magnetic materials. Nine stable magnetic systems are identified. Among them, we find that CrB_4-I, CrB_4-II and CrB_5-I with common structural units [CrB_8] are ferromagnetic metals with estimated T_C of 270 K, 120 K and 110 K, respectively. On the other hand, five CrB_3 phases with structural units [Cr_2B_{12}] are antiferromagnetic metals. Additionally, we also find one antiferromagnetic semiconductor CrB_2-I. Our work may open new directions for identifying 2D magnetic systems with high T_C.

DOI: 10.1088/0256-307X/38/2/027501

Recent decades have witnessed tremendous advances in the research of two-dimensional (2D) materials, stimulated by the successful exfoliation of graphene.[1] Efforts have been made in order to discover novel physics and applications in 2D systems. Among various properties, the magnetism of 2D materials has attracted vast attention for its great promise in spintronic nano-devices.

Initially, researchers tried to realize 2D magnetism based on graphene.[2–4] Because of the weak coupling between the 2p magnetic moments in graphene, transition metal (TM) atoms were introduced to make magnetic interactions more stable.[5,6] However, the d orbitals of TM strongly couple with the valence or the conduction bands of graphene,[7] making it difficult to control the charge or magnetic states. On the other hand, layered transition-metal dichalcogenides (TMDs) such as MoS_2 were considered as candidate materials for spintronic devices due to their sizable bandgaps.[8] Nevertheless, the lack of intrinsic magnetic polarization and magnetic ordering in MoS_2 hinders its applications. Consequently, researchers begin to focus on 2D systems with intrinsic magnetic order, and many 2D magnetic materials were proposed and reported. Among them, monolayer $TMPX_3$ (TM = transition metals, X = chalcogen, S/Se/Te) can exhibit anti-ferromagnetic orders such as Ising antiferromagnetic $FePS_3$[9] and $FePSe_3$,[10] Heisenberg anti-ferromagnetic $MnPS_3$[11] and $MnPSe_3$,[12] and XY anti-ferromagnetic $NiPS_3$.[13] The magnetic order can be further manipulated by tuning the stacking sequences of $TMPX_3$ materials to realize interlayer ferromagnetic order.[14]

In addition to $TMPX_3$, ferromagnetic 2D systems have recently been reported and attracted great attention. These 2D ferromagnetic materials range from semiconductors such as CrI_3[15–18] $Cr_2Ge_2Te_6$[19,20] and $Fe_2Ga_2S_5$[21] to metallic systems including Ni_3GeTe_2[22] and Fe_3GeTe_2.[22–26] However, these 2D intrinsic ferromagnetic materials generally have low Curie temperatures (T_C), thus limiting their application at room temperature. For example, the T_C of monolayer CrI_3, $CrGeTe_3$, and Fe_3GeTe_2 are reported as 61 K,[15] 68 K,[20] and 20 K,[27] respectively. Consequently, there is much hope invested in the discovery or design of novel 2D intrinsic magnetic materials.

Note that the intrinsic magnetic 2D materials often incorporate magnetic elements such as Cr, and non-magnetic elements forming frameworks to host the magnetic elements. While material stability prefers sufficient bonding between Cr and the non-magnetic elements, stable magnetic order requires strong orbital interactions. Apparently, relatively small bond lengths between Cr and the non-magnetic elements would be beneficial. As a result, non-magnetic ele-

Supported in part by the National Key Research and Development Program of China (Grant No. 2016YFB0700700), the National Natural Science Foundation of China (Grant No. 61904035), the Fudan Start-up Funding (Grant No. JIH1512034), and the Shanghai Sailing Program (Grant No. 19YF1403100).
*Corresponding authors. Email: xggong@fudan.edu.cn; jhyang04@fudan.edu.cn

ments with small radii are good candidates to host Cr. Boron, on the left of carbon, naturally meets the above demands. In fact, due to the empty $2p$ orbitals, boron can be quite active and form multi-center and multi-electron bonds in addition to sp^2 and sp^3 hybridization. Two-dimensional materials made of pure boron, known as borophene, have been widely studied both theoretically[28–30] and experimentally[31–33] recently. It has been demonstrated that boron can form very stable and diverse 2D frameworks with coordinate numbers ranging from 3 to 6. Therefore, the combination of magnetic elements with non-magnetic elements such as boron is expected to cultivate novel magnetic systems.[34] In fact, three-dimensional NdFeB magnets were discovered in 1980s.[35] In two-dimensional space, several Cr-based 2D magnetic materials[36–38] have been theoretically proposed with good properties. It is thus of great interest to explore what kinds of magnetic materials boron can form with magnetic elements in 2D space.

In this work, based on the above analysis, we explore the possible formation of 2D chromium borides Cr_xB_y using a differential evolution (DE) algorithm implemented in our self-developed software package IM^{2}ODE,[39] and first-principles calculations. The ratios of Cr and B are set as $x : y = 1 : 2$, $1 : 3$, $1 : 4$ and $1 : 5$ and the total number of atoms is limited to 24, considering our computational resources. Eventually we have identified a total of nine candidates which are stable both energetically and dynamically. Among them, two CrB_4 and one CrB_5 candidates with common structural units [CrB_8] are intrinsic ferromagnetic metals; five planar CrB_3 materials with universal structural units [Cr_2B_{12}] are intrinsic antiferromagnetic metals; one CrB_2 phase is an intrinsic antiferromagnetic semiconductor. The atomic and electronic structures as well as the magnetic properties of the above nine materials are analyzed. The magnetic properties are understood from the Heisenberg model. Using our calculated magnetic exchange interaction parameters, we estimate T_C of CrB_4-I, CrB_4-II and CrB_5-I to be 270 K, 120 K and 110 K, respectively, which are relatively high compared to known 2D magnetic systems. Our work thus will be useful for this emerging field.

Computation Methods—Global Optimization Method for 2D Magnetic Material Design Based on DE. The DE method is one of the global optimization algorithms which can solve the global optimization problem of continuous variables.[40] It is mainly aimed at solving a global search problem that a set of parameters are to be determined, under which the objective function can get the maximum value. In the DE method, each solution case is marked as a D-dimensional vector in which three steps of DE progress are involved: mutation, crossover and selection. For the i^{th} target vector $\boldsymbol{p}_{i,G}$, the mutation operation generates the mutant vector $\boldsymbol{u}_{i,G+1}$ by

$$\boldsymbol{u}_{i,G+1} = \gamma \boldsymbol{p}_{\text{best}} + (1-\gamma)\boldsymbol{p}_{i,G} + F_{\text{D}}(\boldsymbol{p}_{\text{r1}} - \boldsymbol{p}_{\text{r2}}),$$

where G denotes the generation. The random ratio in mutation is controlled by the parameter γ. The best solution in the present generation is $\boldsymbol{p}_{\text{best}}$. Parameter F_{D} manipulates the differential vector; $\boldsymbol{p}_{\text{r1}}$ and $\boldsymbol{p}_{\text{r2}}$ are individuals randomly chosen from the present generation, $r_1 r_2 \in \{1, 2, \ldots, N\}$ and $r_1 \neq r_2 \neq i \neq$ best. In the crossover step, the mutant vector is mixed with the parental vector from the previous generation, so as to create the offspring trial vector $\boldsymbol{p}_{i,G+1} = (\boldsymbol{p}_{1i,G+1}, \boldsymbol{p}_{2i,G+1}, \ldots, \boldsymbol{p}_{\text{D}i,G+1})$ for the next generation, given by

$$\boldsymbol{p}_{ji,G+1} = \begin{cases} \boldsymbol{u}_{ji,G+1}, & \text{if } r(j) \leqslant CR \text{ or } j = rn(i), \\ \boldsymbol{p}_{\text{ji,G}}, & \text{if } r(j) > CR \text{ and } j \neq rn(i), \end{cases}$$

where CR is a constant manually set from 0 to 1 to control the probability of crossover and $r(j)$ is randomly generated within the same range [0,1]. In the selection step of DE progress, we use the greedy principle to determine whether the trial vector $\boldsymbol{p}_{i,G+1}$ is accepted for the next generation. The trial vector $\boldsymbol{p}_{i,G+1}$ is compared with target vector $\boldsymbol{p}_{i,G}$ in the present generation and $\boldsymbol{p}_{i,G+1}$ will not be accepted unless it is better than $\boldsymbol{p}_{i,G}$. In this work, we set $\gamma = 0.20$, $F_{\text{D}} = 0.20$ and $CR = 1.00$.

In materials design, the main objective is to determine the total energy of the structures: the lower the energy, the better the thermodynamic stability. According to the method above, the optimized objective function is

$$\min Z_1 = E_{\text{total}},$$

where the total energy can be given by first-principles calculations. In this work, we use Cr_4B_8 (1:2), Cr_4B_{12} (1:3), Cr_4B_{16} (1:4) and Cr_4B_{20} (1:5) as the basic cells for structural search. In the iteration of differential evolution, we use 30 generations and 30 structures in each generation. Among them, 60% of the structures are generated by the differential evolution algorithm, and the other 40% are randomly generated as mutation seeds.

First-Principles Calculation Methods. The structure optimization and the total energy calculations are performed using density functional theory (DFT) implemented in the VASP code.[41] The magnetic properties are implicitly considered. The projected augmented wave (PAW)[42] method is used to treat ion-electron interactions. For exchange correlations, the PBE method from the generalized gradient approximation (GGA)[43] is adopted. The plane wave cut-off energy is set to be 550 eV. For the integral in the Brillion zone, the Gamma-centered Monkhorst–Pack grid sampling method is selected,[44] and the sampling k point spacing in the reciprocal space is no more than $2\pi \times 0.04\,\text{Å}^{-1}$ for each structure. After obtaining the relaxed structures, we conduct PBE+U[45] calculations to accurately understand the electronic properties of the magnetic systems. For Cr atoms, we set the on-site U parameter as 3.0 eV and the exchange parameter J as 0.9 eV. Other values of U are also tested.

This setting has proven to be effective in other materials in which Cr atoms dominate spin properties, such as $ZnCr_2O_4$.[46] To determine the dynamic stability, phonon spectrum calculations are performed using Phonopy developed by Togo *et al.*[47]

The Energy Mapping Method. The energy mapping method is developed[48] to solve the parameters of magnetic interactions by calculating the energies of various magnetic orders. In this method, a relatively large cell is usually used so that various magnetic structures can be constructed. Here, for simplicity, we use Heisenberg models to describe the spin Hamiltonian because the spin-orbital coupling effects in Cr_xB_y systems are expected to be weak. We consider the nearest and the next-nearest exchange parameters J_1 and J_2 and the spin Hamiltonian is

$$H = J_1 \sum_{i,j}^{n} \hat{S}_i \cdot \hat{S}_j + J_2 \sum_{i,j}^{n} \hat{S}_i \cdot \hat{S}_j.$$

To obtain the value of J_1 and J_2, the energies of three or more structures with different magnetic configurations are calculated and then the exchange parameters J_1 and J_2 can be derived from the energy differences.

Table 1. Formation energy E_{form} per atom of 2D Cr_xB_y($x:y = 1:2$, $1:3$, $1:4$ and $1:5$) systems, the magnetic orders, and the corresponding local magnetic moments of Cr in each material. The formation energy per atom E_{form} is defined as $E_{\text{form}} = \frac{E_{Cr_xB_y} - xE_{Cr} - yE_{Borophene}}{x+y}$, where $E_{Cr_xB_y}$ is the total energy per atom of Cr_xB_y, E_{Cr} and $E_{Borophene}$ are the total energy per atom of pure chromium and synthesized 2D borophene $B_{1/6}$, respectively.

	E_{form} (eV)	Magnetic ground state	Maximal local magnetic moment of Cr (μ_B)
CrB_4-I	−0.2021	FM	2.3
CrB_4-II	−0.1969	FM	2.4
CrB_5-I	−0.1091	FM	2.6
CrB_3-I	−0.1320	AFM	2.6
CrB_3-II	−0.1311	AFM	2.7
CrB_3-III	−0.1252	AFM	2.7
CrB_3-IV	−0.0981	AFM	2.9
CrB_3-V	−0.0974	AFM	2.9
CrB_2-I	−0.1200	AFM	3.0

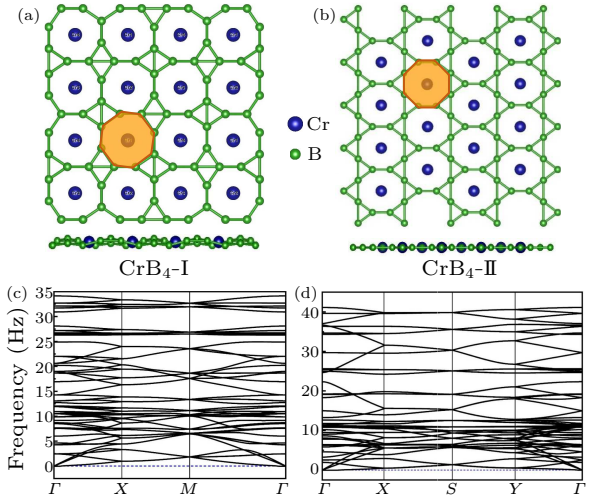

Fig. 1. The atomic structures of searched CrB_4 serial materials in top view (along c-axis) and side view (along a-axis), (a) CrB_4-I and (b) CrB_4-II. Orange regions mark the [CrB_8] units. The [CrB_8] unit forms both candidate CrB_4 structures in different directions or alignments. The phonon spectrum of (c) CrB_4-I and (d) CrB_4-II, respectively.

Results and Discussions. By carrying out the DE structure search and examining the dynamical stabilities, we finally identify nine stable 2D chromium borides without imaginary phonon frequencies. Table 1 shows the formation energies per atom of these structures, the ground magnetic orders, and the local magnetic moments of the Cr atoms.

As we can see, CrB_4-I has the lowest formation energy and thus it is the most stable candidate. Additionally, the formation energy E_{form} of these 2D Cr_xB_y structures are below zero, indicating that they are energetically stable in 2D space and could be synthesized experimentally.

Planar Ferromagnetic Metal CrB_4 Group. First, we discuss the two CrB_4 phases, CrB_4-I and CrB_4-II. Figure 1 shows the atomic structures and corresponding phonon spectra of CrB_4-I and CrB_4-II. As we can see, CrB_4-I is slightly buckled (space group of $P\bar{4}2_1m$) and CrB4-II is purely planar (space group of $Cmmm$). Both the structures are constituent of the basic structural units [CrB_8], in which one Cr atom is surrounded by an octagonal ring of boron atoms. In these two structures, the [CrB_8] units are connected through two boron triangles which share one edge (vertex) and form a diamond (dumbbell). Molecular dynamic simulations performed at $T = 300$ K demonstrate that these structures are thermodynamically stable (see Fig. S1 in the Supplementary Information). To determine the magnetic ground states of CrB_4-I and CrB_4-II, we compare the total energies of various collinear magnetic configurations of Cr atoms in a large supercell. Our results show that both CrB_4-I and CrB_4-II adopt a ferromagnetic (FM) configuration of Cr spins as the ground magnetic order.

Figure 2(a) shows the band structure of FM CrB_4-I, which indicates that CrB_4-I is a metal. The partial charge density distribution near the Fermi level in Fig. 2(b) shows that the Cr orbitals have significant overlap with the orbitals of the nearest B atoms, forming relatively strong bonds and stabilizing the Cr–B network. The density of states in Fig. 2(c) shows that the $d_{3z^2-r^2}$ orbital of Cr is fully occupied while the

d_{xz} and d_{yz} orbitals are partially occupied due to the hybridization with orbitals of B atoms, thus explaining why the local magnetic moments of Cr atoms in CrB_4-I is $2.3\mu_B$ instead of 3 μ_B. To further confirm the FM interactions between Cr atoms, the magnetic exchange parameter is extracted by energy mapping analysis. Figure 2(d) indicates the nearest magnetic exchange parameter J_1 and the next-nearest magnetic exchange parameter J_2 in CrB_4-I. The values of J_1 and J_2 calculated using PBE+U with different U values are listed in Table 2. Note that, in our Heisenberg model, $H = \sum_{i,j}^{n} J_{ij}\hat{S}_i \cdot \hat{S}_j$, the negative exchange parameter J indicates the FM exchange interactions. As we can see, when $U = 3.0$ eV, $J_1 = -33.12$ meV and $J_2 = -0.97$ meV, demonstrating the magnetic interactions between Cr atoms in CrB_4-I are indeed ferromagnetic. With the increase of U, both J_1 and J_2 become more negative, so the ferromagnetic orders do not change. Using the on-site U parameter at $U = 3.0$ eV, we perform Monte Carlo (MC) simulations based on the 2D Heisenberg models and the Curie temperature is estimated to be about 270 K, which is near room temperature and significantly larger than 2D ferromagnetic materials of CrI_3 (61 K) and $CrGeTe_3$ (68 K), suggesting that CrB_4-I could be a practical ferromagnetic system. To further verify the stability of FM state, the magnetic anisotropy energy (MAE) is calculated by considering spin-orbit coupling (SOC) effect. Our results are shown in Table 3. Three representative magnetization directions including (100), (010) and (001) are considered. Our results show that the easy axis of CrB_4-I is along (001) direction and perpendicular to the Cr–B plane. The calculated MAE is 338.4 μeV per Cr atom, which is much larger than that of Fe (−1.4 μeV) and Co (−65 μeV).[49] Different U parameters ranging from 3.0 eV to 5.0 eV are tested and our conclusion still holds. The large MAE indicates that the FM states are stable against spin cantings.

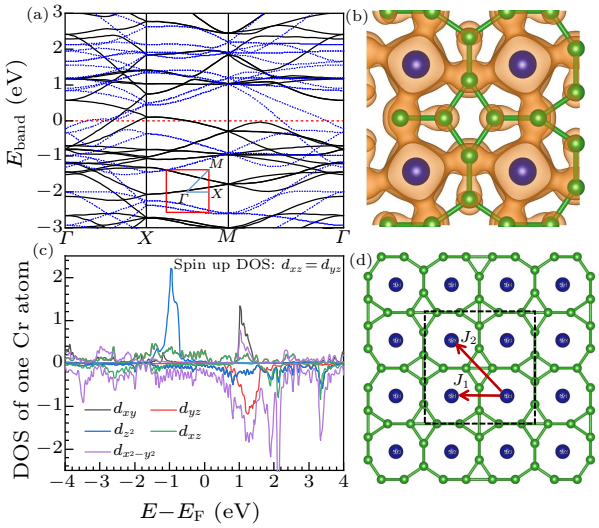

Fig. 2. (a) The band structure of FM CrB_4-I. The black solid lines and the blue dotted lines show the spin-up and spin-down bands, respectively. The red dotted line shows the Fermi energy level E_F, and the high symmetric point path in the Brillouin region is shown internally. (b) The charge density between E_F and $E_F-2.0$ eV in FM CrB_4-I. (c) The d-orbital-projected DOS of one Cr atom in FM CrB_4-I. (d) The calculated magnetic interaction parameters J_1 and J_2 in FM CrB_4-I.

Table 2. The calculated nearest exchange parameter J_1 and the next-nearest magnetic exchange parameter J_2 in FM CrB_4-I, CrB_4-Ⅱ, and CrB_5-I using the PBE+U method.

		$U = 3.0$ eV	$U = 4.0$ eV	$U = 5.0$ eV
CrB_4-I	J_1 (meV)	−33.12	−37.03	−40.72
	J_2 (meV)	−0.97	−1.55	−2.31
CrB_4-Ⅱ	J_1 (meV)	−27.49	−28.39	−28.76
	J_2 (meV)	−2.99	+2.40	+2.94
CrB_5-I	J_1 (meV)	−27.07	−22.18	−13.12
	J_2 (meV)	−20.33	−20.42	−19.58

Table 3. The calculated MAE of FM CrB_4-I, CrB_4-Ⅱ and CrB_5-I with different settings of the on-site U parameters. The easy axis is also indicated.

		$E_{100} - E_{001}$ per Cr atom (μeV)	$E_{010} - E_{001}$ per Cr atom (μeV)	Easy axis
CrB_4-I	$U = 3.0$ eV	338.4	336.8	(001)
	$U = 4.0$ eV	324.0	323.5	(001)
	$U = 5.0$ eV	337.2	337.8	(001)
CrB_4-Ⅱ	$U = 3.0$ eV	306.4	555.9	(001)
	$U = 4.0$ eV	267.6	518.5	(001)
	$U = 5.0$ eV	284.5	455.1	(001)
CrB_5-I	$U = 3.0$ eV	332.8	350.3	(001)
	$U = 4.0$ eV	336.8	348.6	(001)
	$U = 5.0$ eV	346.7	342.2	(001)

CrB_4-Ⅱ has very similar electronic and magnetic properties as CrB_4-I, i.e., it is also a metal [Fig. 3(a)] and has large orbital overlap near the Fermi level between the Cr and the nearest B atoms [Fig. 3(b)]. Orbital hybridization leads to the local magnetic moment of each atom being about $2.4\mu_B$ (see Table 1). The $d_{3z^2-r^2}$ orbital of Cr atoms is fully occupied while the d_{xz} and d_{yz} orbitals are partially occupied [Fig. 3(c)]. The calculated magnetic interaction parameters are $J_1 = -27.49$ meV and $J_2 = -2.99$ meV at $U = 3.0$ eV, demonstrating the FM exchange interactions. With the increase of U, J_1 slightly decreases while J_2 becomes slightly positive. Nevertheless, the nearest ferromagnetic interaction is much stronger than the next-nearest magnetic interaction. Consequently, the change of U parameters does not change the FM ordering in CrB_4-Ⅱ. Using the calculated parameters at $U = 3.0$ eV, the Curie temperature estimated by MC

simulation is about 120 K, still larger than that of CrI_3 and $CrGeTe_3$. Our further calculations of MAE show that the easy axis of CrB_4-Ⅱ is along (001) direction and the large MAE of 306.4 μeV per Cr atom demonstrates the robustness of the FM states.

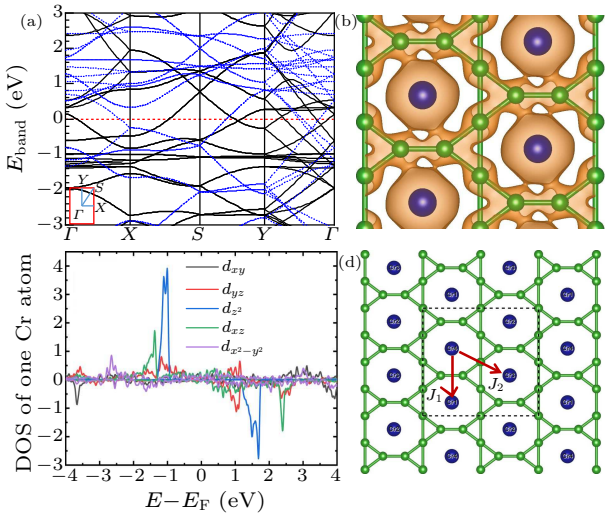

Fig. 3. (a) The band structure of FM CrB_4-Ⅱ. The black solid lines and the blue dotted lines show the spin-up and spin-down bands, respectively. The red dotted line shows the Fermi energy level, and the high symmetric point path in the Brillouin region is shown internally. (b) The charge density between E_F and $E_F-2.0$ eV in FM CrB_4-Ⅱ. (c) The d-orbital-projected DOS of one Cr atom in FM CrB_4-Ⅱ. (d) The calculated magnetic interaction parameter J_1 and J_2 in FM CrB_4-Ⅱ.

Quasi-Planar Ferromagnetic Metal CrB_5-I. In addition to CrB_4-I and CrB_4-Ⅱ, we also find that CrB_5-I, composed of the same $[CrB_8]$ units, is ferromagnetic as well. The atomic structure of CrB_5-I is shown in Fig. 4(a), which is slightly buckled with a space group of *Pba*2. Different from CrB_4-I and CrB_4-Ⅱ in which the $[CrB_8]$ units are in parallel alignment, the $[CrB_8]$ units in CrB_5-I are twisted and connected through triangular boron networks. Phonon calculations in Fig. 4(b) and molecular dynamic simulations in Fig. S2 indicate that CrB_5-I is both dynamically and thermodynamically stable. We note that, CrB_4-I, CrB_4-Ⅱ, and CrB_5-I can be seen as eliminating certain boron atoms in vacancy-free boron sheets and then doping Cr atoms with tiny relaxation, which could be a routine path to synthesize them.

The band structure of CrB_5-I is given in Fig. 4(c), showing that CrB_5-I is metallic. The density of states in Fig. 4(d) shows the occupied $d_{3z^2-r^2}$ orbitals and partially occupied d_{xz} and d_{yz} orbitals of Cr atoms below the Fermi level. The hybridization between Cr orbitals and B orbitals results in the local magnetic moments of $2.6\mu_B$ (see Table 1).

For the magnetic properties, we calculate the Heisenberg nearest exchange parameter J_1 and the next-nearest magnetic exchange parameter J_2 [see Fig. 4(a)] for CrB_5-I. As seen in Table 2, both J_1 and J_2 are very negative for $U = 3.0$ eV, 4.0 eV, and 5.0 eV, respectively, supporting the strong FM exchange interactions in CrB_5-I. Using J values at $U = 3.0$ eV, we estimate the Curie temperature by MC simulation to be about 110 K, still larger than those of CrI_3 and $CrGeTe_3$. Similar to CrB_4-I and CrB_4-Ⅱ, CrB_5-I also has a large MAE of 332.8 μeV per Cr atom along (001) direction. We note that the Curie temperatures decrease from CrB_4-I to CrB_4-Ⅱ and then to CrB_5-I. This is because the nearest exchange parameters dominate the magnetic order.

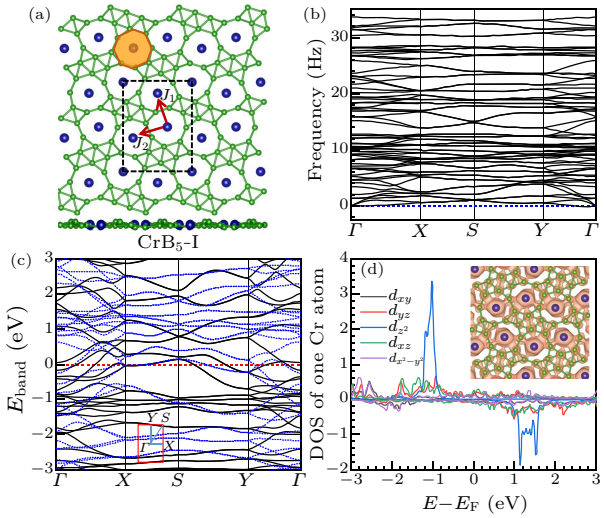

Fig. 4. (a) The atomic structure of FM CrB_5-I. Orange region marks the $[CrB_8]$ unit. The red vectors mark the directions of calculated magnetic interaction parameters J_1 and J_2 in FM CrB_5-I. (b) The phonon spectrum of FM CrB_5-I. (c) The band structure of FM CrB_5-I. The black solid lines and the blue dotted lines show the spin-up and spin-down bands, respectively. The red dotted line shows the Fermi energy level, and the high symmetric point path in the Brillouin region is shown internally. (d) The d-orbital-projected DOS of one Cr atom in FM CrB_5-I. The inner figure shows the charge density between E_F and $E_F-2.0$ eV in FM CrB_5-I.

Planar Antiferromagnetic Metal CrB_3 Series. Besides the above three ferromagnetic metallic systems, we also identify 6 antiferromagnetic 2D chromium borides, including five CrB_3 metallic phases and one CrB_2 semiconducting phase. Figure 5 shows the atomic structures of CrB_3 series, all of which are purely planar. In general, the five CrB_3 phases can be seen as formed by the structural unit $[Cr_2B_{12}]$, which consists of two merging octagonal boron rings with the B–B bond at the sharing edge broken due to the strain effect. The structural differences among these five CrB_3 phases lie in the direction and alignment orders of $[Cr_2B_{12}]$ units.

Taking CrB_3-I [see Figs. 5(a) and 6(a)], which has the most stable phase of CrB_3, as a typical example, we present its electronic and magnetic properties. Figure 6(b) shows the calculated phonon spectrum of CrB_3-I. The absence of imaginary frequencies indicates its dynamical stability. The stability of other CrB_3 systems is demonstrated by phonon calculations and molecular dynamics simulations, which are provided in Figs. S3 and S6 in the Supplemen-

tary Information, respectively. Both the band structure [Fig. 6(c)] and the density of states [Fig. 6(d)] show that CrB_3-I is an antiferromagnetic metal. Detailed analysis shows that the AFM configuration exists within the structural unit $[Cr_2B_{12}]$.

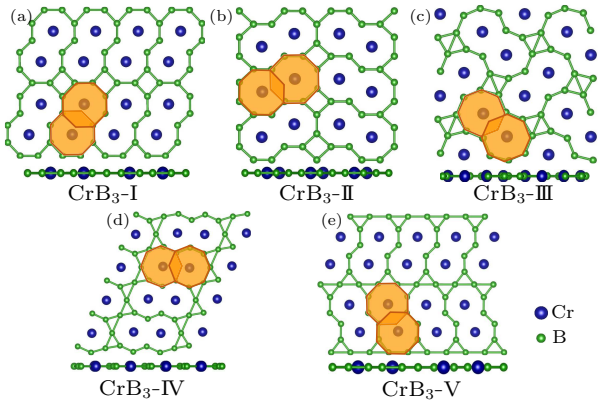

Fig. 5. The atomic structures of searched CrB_3 series in top view (along c-axis) and side view (along a-axis) for CrB_3-I–V (a)–(e). Orange regions mark the $[Cr_2B_{12}]$ units. The $[Cr_2B_{12}]$ unit forms all candidate CrB_3 structures in different directions or alignments.

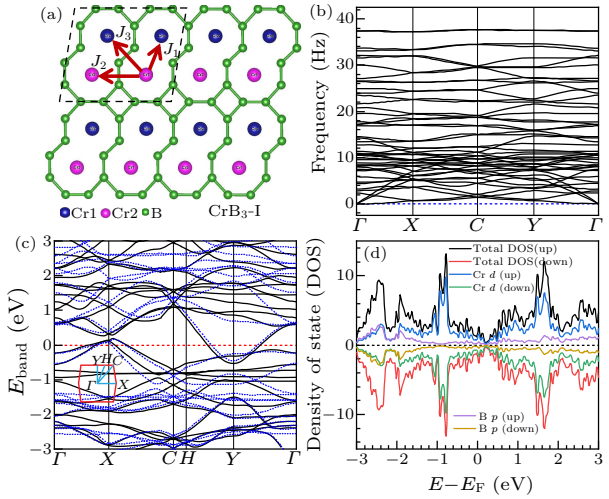

Fig. 6. (a) Magnetic ground state AFM CrB_3-I. Blue and pink balls show the Cr1 and Cr2 atoms with antiparallel spin. The red vectors mark the directions of calculated magnetic interaction parameters J_1, J_2 and J_3 in AFM CrB_3-I. (b) The phonon spectrum of CrB_3-I. (c) The band structure of AFM CrB_3-I. The black solid lines show the PBE band, the blue dotted lines show the PBE+U band, the red dotted line shows the Fermi energy level and the high symmetric point path in the Brillouin region is shown internally. (d) The projected DOS of CrB_3-I.

As can be seen in Fig. 6(a), the spins of the two Cr atoms in one structural unit are anti-parallel to each other. However, the Cr atoms in two neighboring structural units will have the same spin direction if they are at the same location of their structural unit. The same magnetic orders also exist in the other CrB_3 phases (see Fig. S4 in the Supplementary Information). The calculated nearest exchange parameter $J_1 = +0.99$ meV, next-nearest exchange parameter $J_2 = -6.18$ meV, and next-next-nearest exchange parameter $J_3 = +4.74$ meV, agree with the above antiferromagnetic orders.

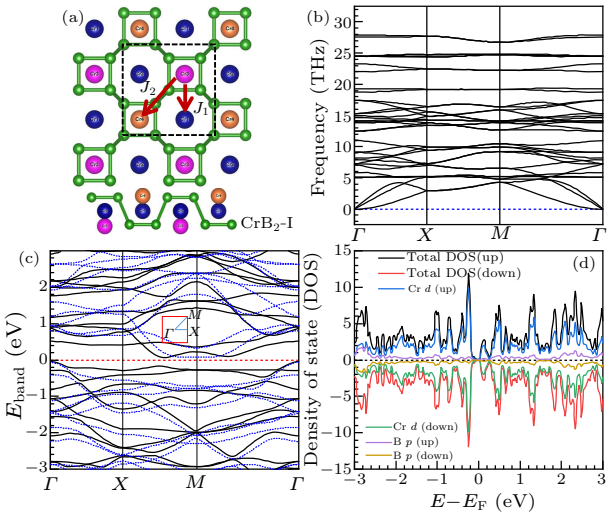

Fig. 7. (a) Magnetic ground state G-type AFM CrB_2-I. Blue balls show the Cr1 atoms without a local magnetic moment, pink balls show the Cr2 atoms with up-spin, and orange balls show the Cr3 atoms with down-spin. (b) The phonon spectrum of CrB_2-I. (c) The band structure of G-type AFM CrB_2-I. The black solid lines show the PBE band, the blue dotted lines show the PBE+U band, the red dotted line shows the Fermi energy level, and the high symmetric point path in the Brillouin region is shown internally. (d) The projected DOS of CrB_2-I.

Antiferromagnetic Semiconductor CrB_2-I. In addition to the antiferromagnetic metals, we also identify one semiconducting phase CrB_2-I. The lattice structure of CrB_2-I is given in Fig. 7(a) with a space group of $P4/nmm$. As we can see, the primitive cell contains four Cr atoms and eight B atoms. The boron framework consists of a quasi-two-dimensional arrangement of two sublayers, in each of which boron forms squares with bond lengths of 1.75 Å. The B–B bonds connecting the two sublayers have lengths of 2.04 Å. The four interlayer B–B bonds and four intra-layer B–B bonds (two bonds in each sublayer) form rugged octagons. The Cr atoms in the boron framework are divided into three categories: Cr1 is at the octagon center and located in the middle of two boron sublayers; Cr2 is under the boron square in the upper layer; Cr3 is above the boron square in the lower layer. The Cr–B forms a unique arrangement similar to a chess board. The dynamic stability of CrB_2-I is confirmed with imaginary-free phonon modes [see Fig. 7(b)].

In order to reveal the magnetic ground state of CrB_2-I, we enumerate different spin directions of the four Cr atoms in the primitive cell. Our results show that different initial spin configurations eventually converge to three situations, including FM (each Cr atom spin lies in the same direction), NM (all local magnetic moments of Cr atoms are annihilated), and G-type AFM (each Cr2 atom has opposite spin directions to its neighboring Cr3 atoms and vice versa). However, the FM and NM configurations have total energies of 228 meV and 48 meV per formula unit (f.u.)

higher than the G-type AFM state, respectively. As a result, we conclude that G-type AFM is the magnetic ground state configuration of CrB_2-I. We further calculate the magnetic exchange parameters and the values are $J_1 = -2.24$ meV and $J_2 = 3.44$ meV, supporting the G-type AFM magnetic order.

The band structure of G-type AFM CrB_2-I using PBE+U with a U value of 3.0 eV is shown in Fig. 7(c). The calculated band gap show that CrB_2-I is a narrow-band semiconductor with an indirect band gap of $E_g = 0.14$ eV. Density of states in Fig. 7(d) shows that the 3d orbital of the Cr atom dominates at both the valance band maximum (VBM) and the conduction band minimum (CBM).

In conclusion, based on our self-developed software package IM^{2}ODE, we have identified nine 2D chromium borides which are stable energetically and dynamically, including intrinsic FM metals (CrB_4-I, CrB_4-Ⅱ and CrB_5-I), intrinsic AFM metals (five CrB_3 phases) and one intrinsic AFM semiconductors (CrB_2-I). The structures, electronic structures, and magnetic properties have been investigated. Using the Heisenberg model, we have explained the magnetic interactions in these systems and estimated the T_C of CrB_4-I, CrB_4-Ⅱ and CrB_5-I to be 270 K, 120 K and 110 K, respectively, which are relatively high compared to known 2D magnetic systems. Our work is expected to be useful for this emerging field and may open new directions of searching novel 2D magnetic materials.

Supplementary Information. Molecular dynamical simulation results for CrB_3-I/Ⅱ/Ⅲ/Ⅳ/V, CrB_4–I/Ⅱ and CrB_5-I at $T = 300$ K, the magnetic ground states and the electronic structures of CrB_3-Ⅱ/Ⅲ/Ⅳ/V, the electronic structures of CrB_3-Ⅱ/Ⅲ/Ⅳ/V and the Monte-Carlo simulations of the Curie temperatures of CrB_4-I, CrB_4-Ⅱ and CrB_5-I.

The calculations are performed at the High-Performance Computing Center of Fudan University. We thank Dr. Xu Ke at Hubei University of Arts and Science, Dr. Feng Junsheng at Anhui Normal University, Dr. Hou Yusheng at Sun-Yat-sen University, and Miss Wu Na in Department of Chemistry, Fudan University, for useful discussions.

References

[1] Novoselov K S, Geim A K, Morozov S V, Jiang D, Zhang Y, Dubonos S V, Grigorieva I V and Firsov A A 2004 *Science* **306** 666
[2] Tao C, Jiao L, Yazyev O V, Chen Y, Feng J, Zhang X, Capaz R B, Tour J M, Zettl A and Louie S G 2011 *Nat. Phys.* **7** 616
[3] Ugeda M M, Brihuega I, Guinea F and Gómez-Rodríguez J M 2010 *Phys. Rev. Lett.* **104** 96804
[4] Tombros N, Jozsa C, Popinciuc M, Jonkman H T and Van Wees B J 2007 *Nature* **448** 571
[5] Sielemann R, Kobayashi Y, Yoshida Y, Gunnlaugsson H P and Weyer G 2008 *Phys. Rev. Lett.* **101** 137206
[6] Karpan V M, Giovannetti G, Khomyakov P A, Talanana M, Starikov A A, Zwierzycki M, Van Den Brink J, Brocks G and Kelly P J 2007 *Phys. Rev. Lett.* **99** 176602
[7] Krasheninnikov A V, Lehtinen P O, Foster A S, Pyykkö P and Nieminen R M 2009 *Phys. Rev. Lett.* **102** 126807
[8] Radisavljevic B, Radenovic A, Brivio J, Giacometti V and Kis A 2011 *Nat. Nanotechnol.* **6** 147
[9] Lee J, Lee S, Ryoo J H, Kang S, Kim T Y, Kim P, Park C, Park J and Cheong H 2016 *Nano Lett.* **16** 7433
[10] S S M, Jouanne M, Balkanski M, Ouvrard G and Benedek G 1987 *Phys. Rev. B* **35** 7097
[11] Sun Y, Tan Q, Liu X, Gao Y and Zhang J 2019 *J. Phys. Chem. Lett.* **10** 3087
[12] Li X, Wu X and Yang J 2014 *J. Am. Chem. Soc.* **136** 11065
[13] Joy P A and Vasudevan S 1992 *Phys. Rev. B* **46** 5425
[14] Ressouche E, Loire M, Simonet V, Ballou R, Stunault A and Wildes A 2010 *Phys. Rev. B* **82** 100408
[15] Huang B, Clark G, Navarro-Moratalla E, Klein D R, Cheng R, Seyler K L, Zhong D, Schmidgall E, McGuire M A and Cobden D H 2017 *Nature* **546** 270
[16] McGuire M A, Dixit H, Cooper V R and Sales B C 2015 *Chem. Mater.* **27** 612
[17] Wang J, Huang J, Wang Y, Yang T and Zhang Z 2019 *Chin. Phys. B* **28** 77301
[18] Guo Y, Liu N, Zhao Y, Jiang X, Zhou S and Zhao J 2020 *Chin. Phys. Lett.* **37** 107506
[19] Li X and Yang J 2014 *J. Mater. Chem. C* **2** 7071
[20] Gong C, Li L, Li Z, Ji H, Stern A, Xia Y, Cao T, Bao W, Wang C and Wang Y 2017 *Nature* **546** 265
[21] Liao C, Jin Y, Zhang W, Zhu Z and Chen M 2020 *Chin. Phys. Lett.* **37** 107505
[22] Deiseroth H J, Aleksandrov K, Reiner C, Kienle L and Kremer R K 2006 *Eur. J. Inorg. Chem.* **2006** 1561
[23] Zhu J, Janoschek M, Chaves D S, Cezar J C, Durakiewicz T, Ronning F, Sassa Y, Mansson M, Scott B L and Wakeham N 2016 *Phys. Rev. B* **93** 144404
[24] May A F, Calder S, Cantoni C, Cao H and McGuire M A 2016 *Phys. Rev. B* **93** 14411
[25] Xu J, Wang S, Wang W, Zhou Y, Chen X, Yang Z and Qu Z 2020 *Chin. Phys. Lett.* **37** 076202
[26] Chen X, Lin Z Z and Cheng L R 2020 *Chin. Phys. B* **30** (in press)
[27] Deng Y, Yu Y, Song Y, Zhang J, Wang N Z, Sun Z, Yi Y, Wu Y Z, Wu S, Zhu J 2018 *Nature* **563** 94
[28] Zhang Z, Yang Y, Gao G and Yakobson B I 2015 *Angew. Chem.* **127** 13214
[29] Zhang Z, Penev E S and Yakobson B I 2017 *Chem. Soc. Rev.* **46** 6746
[30] Zhang Z, Yang Y, Penev E S and Yakobson B I 2017 *Adv. Funct. Mater.* **27** 1605059
[31] Zhang Z, Mannix A J, Liu X, Hu Z, Guisinger N P, Hersam M C and Yakobson B I 2019 *Sci. Adv.* **5** eaax0246
[32] Mannix A J, Zhang Z, Guisinger N P, Yakobson B I and Hersam M C 2018 *Nat. Nanotechnol.* **13** 444
[33] Liu L, Zhang Z, Liu X, Xuan X, Yakobson B I, Hersam M C and Guo W 2020 *Nano Lett.* **20** 1315
[34] Xie A, Wen T and Li J 2019 *Chin. Phys. Lett.* **36** 117302
[35] Mishra R K 1987 *J. Appl. Phys.* **62** 967
[36] Guo Y, Zhang Y, Yuan S, Wang B and Wang J 2018 *Nanoscale* **10** 18036
[37] Miao N, Xu B, Zhu L, Zhou J and Sun Z 2018 *J. Am. Chem. Soc.* **140** 2417
[38] Telford E J, Dismukes A H, Lee K, Cheng M, Wieteska A, Bartholomew A K, Chen Y, Xu X, Pasupathy A N, Zhu X, Dean C R and Roy X 2020 *Adv. Mater.* **32** 2003240
[39] Zhang Y, Gao W, Chen S, Xiang H and Gong X 2015 *Comput. Mater. Sci.* **98** 51
[40] Storn R and Price K 1997 *J. Global Optim.* **11** 341
[41] Kresse G and Hafner J 1994 *Phys. Rev. B* **49** 14251
[42] Blöchl P E 1994 *Phys. Rev. B* **50** 17953
[43] Perdew J P, Burke K and Ernzerhof M 1996 *Phys. Rev. Lett.* **77** 3865
[44] Monkhorst H J and Pack J D 1976 *Phys. Rev. B* **13** 5188
[45] Liechtenstein A I, Anisimov V I and Zaanen J 1995 *Phys. Rev. B* **52** R5467
[46] Fennie C J, Rabe K M 2006 *Phys. Rev. Lett.* **96** 205505
[47] Togo A and Tanaka I 2015 *Scr. Mater.* **108** 1
[48] Zhou Y, Geng W and Wang D 1998 *Phys. Rev. B* **57** 5029
[49] Daalderop G, Kelly P J and Schuurmans M 1990 *Phys. Rev. B* **41** 11919

Supplementary Information for

"Rational Design of Two-dimensional Magnetic Chromium Borides from First-principles"

Zhang Yi-Lin(张奕林)[1,2], Zhang Yue-Yu(张越宇)[3], Ni Jin-Yang(倪斤阳)[1,2], Yang Ji-Hui(杨吉辉)[1,2*], Xiang Hong-Jun(向红军)[1,2], and Gong Xin-Gao(龚新高)[1,2*]

[1]Key Laboratory of Computational Physical Sciences (Ministry of Education), State Key Laboratory of Surface Physics, and Department of Physics, Fudan University, Shanghai 200433, P. R. China

[2] Collaborative Innovation Center of Advanced Microstructures, Nanjing 210093, P. R. China

[3] Department of Chemistry, Imperial College London, W12 0BZ, United Kingdom

E-mail: xggong@fudan.edu.cn; jhyang04@fudan.edu.cn

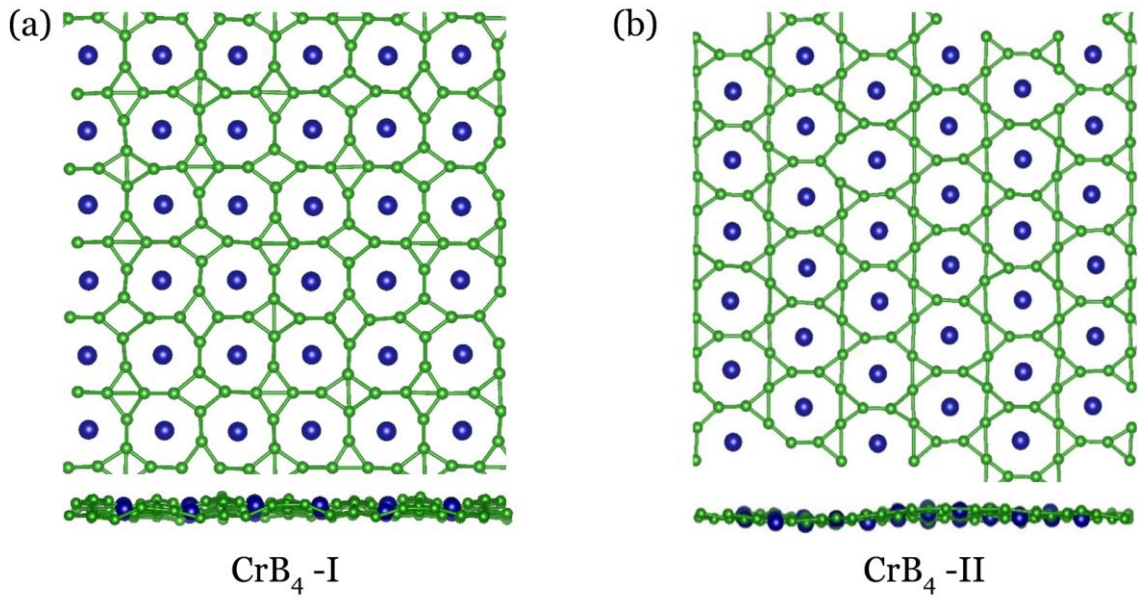

Figure S1. Snapshots of molecular dynamics simulations of (a) CrB_4-I and (b) CrB_4-II, T=300K.

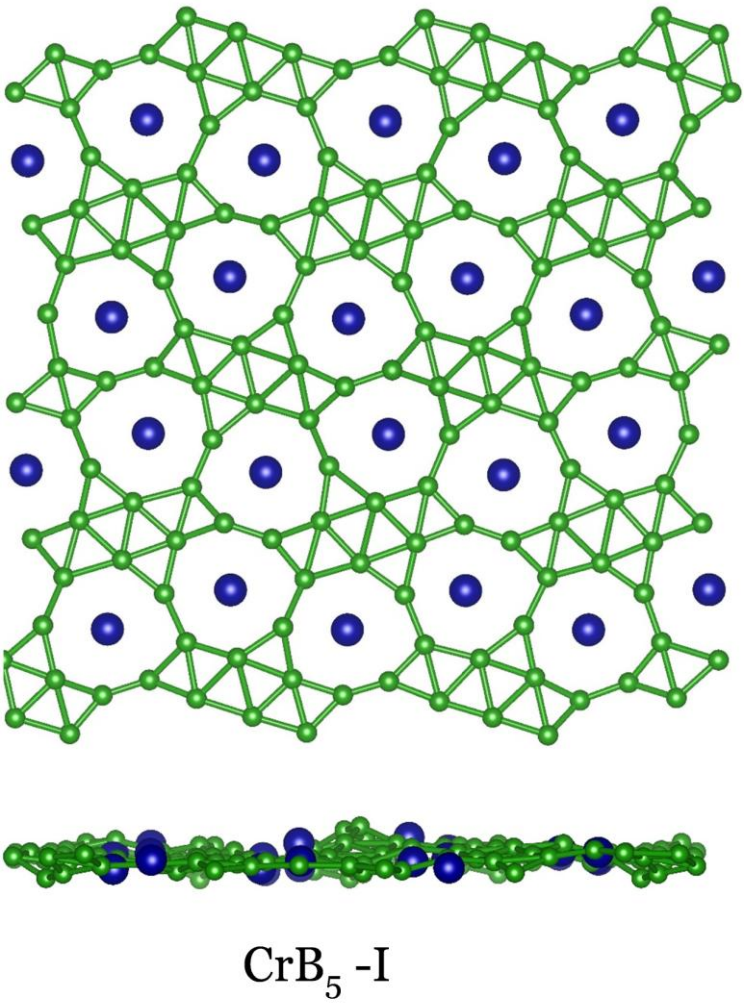

Figure S2. Snapshots of molecular dynamics simulations of CrB_5-I, T=300K.

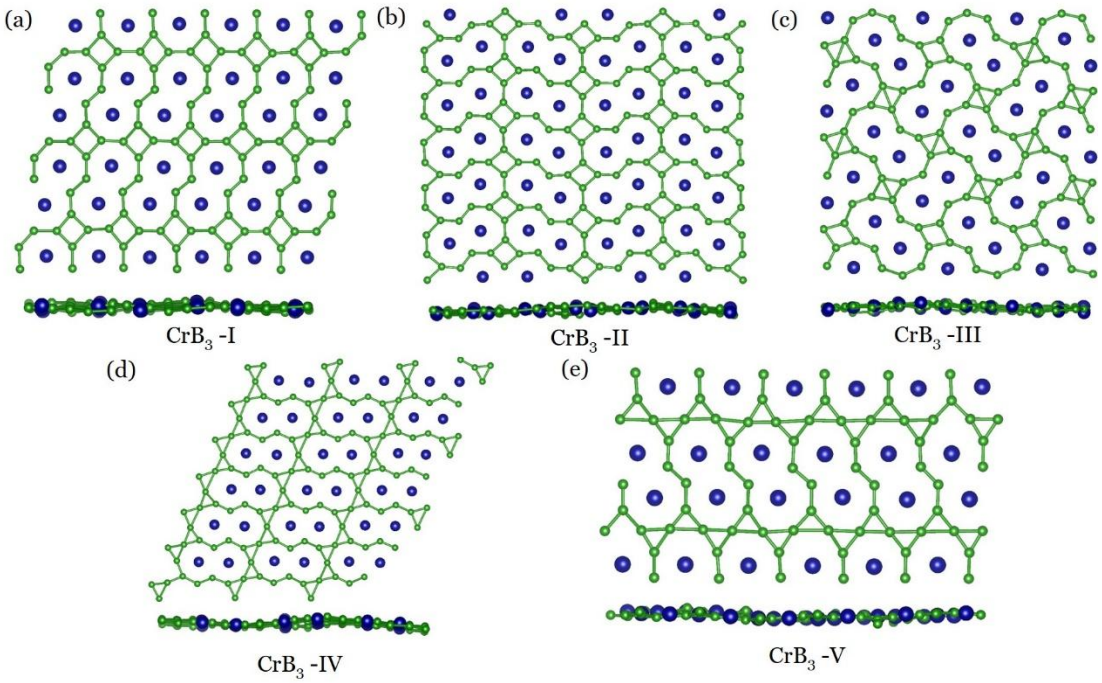

Figure S3. Snapshots of molecular dynamics simulations of CrB_3 series, T=300K. (a)-(e) for CrB_3-I~V, respectively

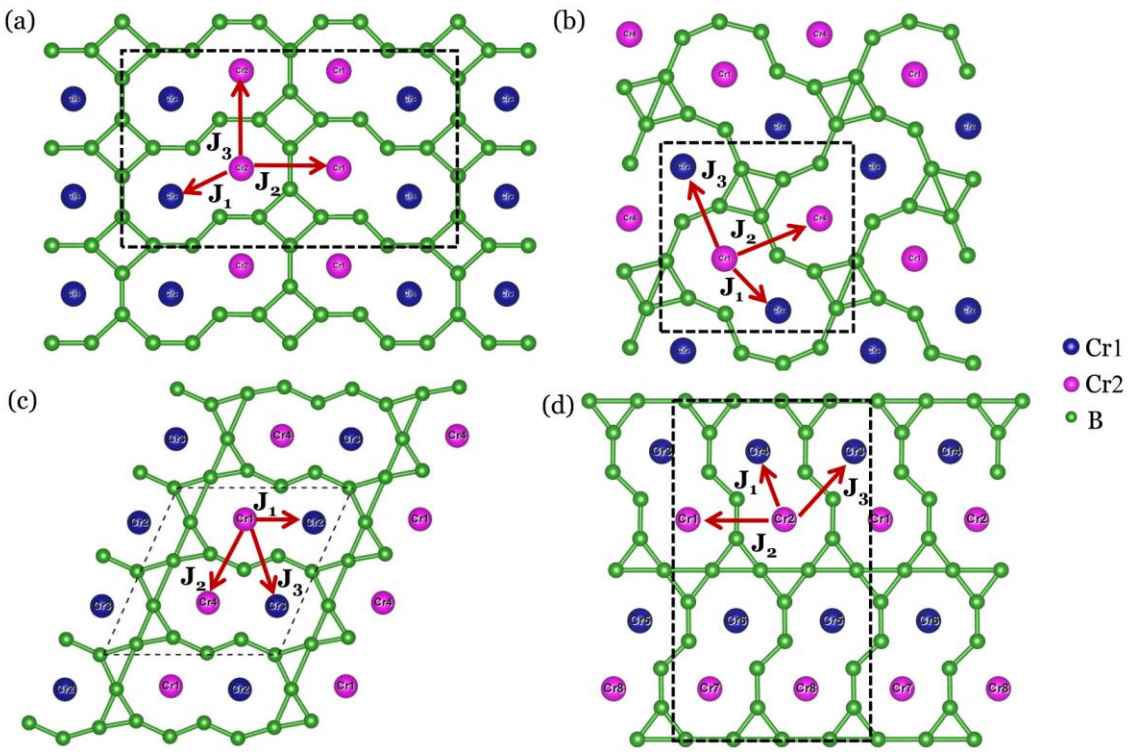

Figure S4. Scheme of antiferromagnetic configurations for (a) CrB_3-II, (b) CrB_3-III, (c) CrB_3-IV and (d) CrB_3-V. Blue and pink balls show the Cr1 and Cr2 atoms with antiparallel spin. The spin of the two Cr atoms in one structural unit is anti-parallel to each other, while for two neighbouring structural units, Cr atoms in corresponding location have same direction of spin. The red vectors mark the directions of calculated magnetic interaction parameters $\boldsymbol{J_1}$, $\boldsymbol{J_2}$ and $\boldsymbol{J_3}$.

		U=3.0eV	U=4.0eV	U=5.0eV
CrB_3-I	J_1 /meV	0.99	1.34	2.34
	J_2 /meV	-6.18	-5.88	-5.35
	J_3 /meV	4.74	4.68	4.64
CrB_3-II	J_1 /meV	8.74	10.61	8.90
	J_2 /meV	-6.75	-7.45	-4.02
	J_3 /meV	-5.51	-6.07	-4.49
CrB_3-III	J_1 /meV	7.06	7.10	7.43
	J_2 /meV	-2.43	-2.07	-1.34
	J_3 /meV	3.53	3.55	3.71
CrB_3-IV	J_1 /meV	13.36	10.77	14.48
	J_2 /meV	-9.37	-6.98	-7.01
	J_3 /meV	4.38	2.84	5.63
CrB_3-V	J_1 /meV	6.44	7.38	9.54
	J_2 /meV	-8.56	-6.89	-4.49
	J_3 /meV	-1.19	-0.78	-0.23
CrB_2-I	J_1 /meV	-2.24	-1.93	-2.22
	J_2 /meV	3.44	3.73	3.94

Table S1. The magnetic exchange parameters J_1, J_2 and J_3 of CrB_3-II/III/IV/V and CrB_2-I under various PBE+U method with Hubbard-U of 3.0, 4.0 and 5.0 eV, derived from energy mapping analysis.

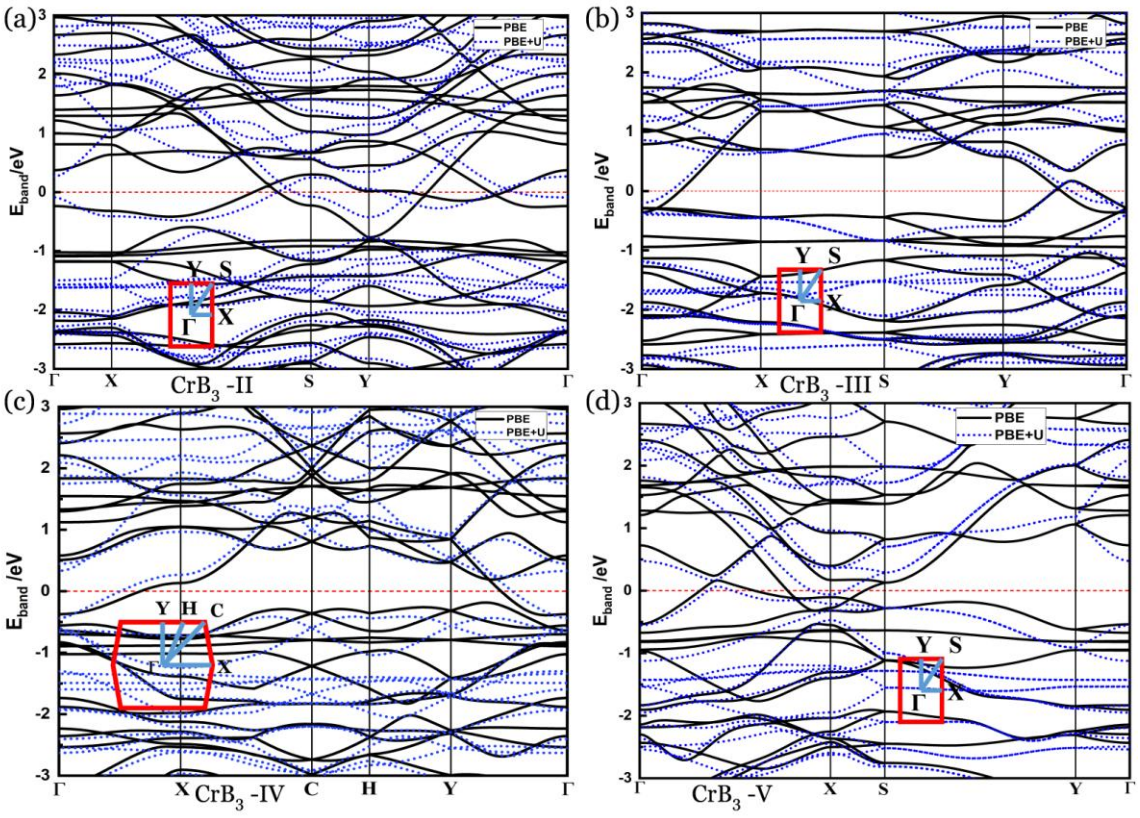

Figure S5. The band structures of AFM CrB_3-II/III/IV/V. The black solid lines show the PBE band, the blue dotted lines show the PBE+U band. The red dotted line shows the Fermi energy level, and the high symmetric point path in the Brillouin region is shown internally.

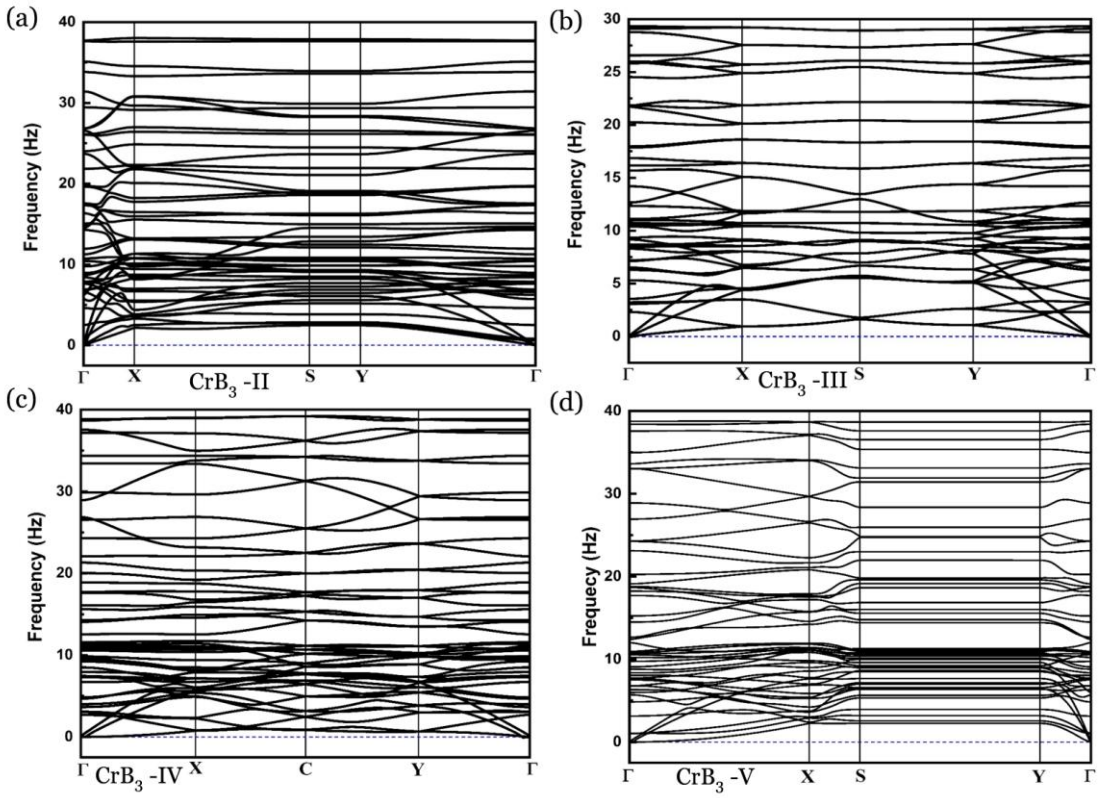

Figure S6. The phonon spectra of AFM CrB_3-II/III/IV/V.